ELSEVIER

Direct and large-eddy simulation of turbulent fluid flow using the lattice-Boltzmann scheme

Jack G. M. Eggels
Shell International Oil Products B. V., Shell Research and Technology Centre, Amsterdam, The Netherlands

This paper reports on direct and large-eddy simulations (LES) of turbulent flows using the lattice-Boltzmann scheme for the discretization of the Navier-Stokes equations. It is divided into two parts. The first part deals with direct simulation of fully developed turbulent channel flow with heat transfer in order to check the performance of our solver. It is shown that the present numerical results agree well with the numerical results reported by Kim et al. (1987). The second part deals with large-eddy simulation (LES) of the turbulent flow in a baffled stirred tank reactor. This kind of equipment is frequently used in the (petro)chemical industry for mixing applications and is, therefore, of direct practical relevance. Large-eddy simulation is a powerful tool to study such flows, as it accounts in a natural way for the unsteady and quasi-periodic behavior of these flows. The results of our first attempt to simulate this flow by means of modeling the impact of the mechanical impeller on the flow field via a varying force field in space and time, reveal a fair agreement with available experimental data. In accordance with measurements, it is shown that the thickness of the impeller blades plays an important role for the motion of the fluid in the vicinity of the impeller. In conclusion, the present application of LES to this engineering flow problem clearly shows the potential of LES as a tool to investigate turbulent flows in industrial applications of practical importance.

Keywords: direct and large-eddy simulation; lattice-Boltzmann scheme; fully developed channel flow; stirred tank reactors

Introduction

The lattice-Boltzmann scheme, and the closely related lattice-gas automata, are a particular class of numerical techniques used to solve the equations of motion for a time-dependent fluid flow. The first really successful lattice-gas automaton was introduced by Frisch, Hasslacher and Pomeau for the simulation of the two-dimensional (2-D) incompressible Navier–Stokes equations (Frisch et al. 1986). Since then, many variants have been proposed; e.g., for the simulation of three-dimensional (3-D) flow, multiphase flow, compressible flow, and non-Newtonian flow. Several nontrivial applications have been reported by Somers and Rem (1991). Extensions of the scheme to enable simulations of thermal flows have been published recently by Massaioli et al. (1993) and Eggels and Somers (1995). The purpose of the lattice-Boltzmann project at Shell Research is to develop a computational tool based on the lattice-Boltzmann scheme with which direct and large-eddy simulations (LES) of industrially relevant flow problems can be performed. The reasons for selecting this particular technique are multiple. First, the lattice-Boltzmann scheme can easily handle the complex geometries which are almost always encountered in industrial applications. Second, the method is efficient from a computational point of view in the sense that the number of operations per gridpoint is smaller than for other methods, such as finite difference schemes. Furthermore, solving (macroscopic) partial differential equations other than the Navier–Stokes equations in the lattice-Boltzmann framework is feasible with only a small effort. Finally, due to the strongly local character of the scheme (the local, grid point based, collision step of the scheme is more time-consuming than the global propagation step, see Eggels and Somers 1995), it is an attractive scheme to run on parallel computer platforms.

This paper first reports on a validation study considering fully developed turbulent channel flow with heat transfer between two parallel plates. To check the performance of our solver without the influence of a subgrid-scale (SGS) turbulence model, all scales of turbulent motion are fully resolved in space and time in these simulations. The results of this direct numerical simulation (DNS) are compared with those reported by Kim et al. (1987). Next, the isothermal, single-phase, turbulent flow in a baffled stirred tank reactor (BSTR) is considered using LES. This kind of equipment is frequently used in the (petro)chemical industry and detailed information on the (time-dependent) flow patterns

Address reprint requests to Dr. Jack G. M. Eggels, Attn: H. Hendriks, Shell Research and Technology Centre, P.O. Box 38000, 1030 BN Amsterdam, The Netherlands.

Received 13 October 1995; accepted 17 February 1996

Int. J. Heat and Fluid Flow 17: 307–323, 1996

655 Avenue of the Americas, New York, NY 10010

0142-727X/96/$15.00
PII S0142-727X(96)00044-9

in such reactors is important for an optimal design. As a first attempt to simulate the flow in these reactors, the "real" practical flow problem is largely simplified by considering a single-phase, isothermal, Newtonian fluid. Despite these simplifications, the results of this study already provide insight into the flow patterns occurring in such systems. Profiles of mean and fluctuating velocities for a system agitated by a standard disc turbine are presented and compared to experimental data.

In the author's opinion, the full details of the lattice-Boltzmann scheme are beyond the scope of the present paper. For reference see Eggels and Somers (1995), McNamara and Zanetti (1989), Succi et al. (1992) and Chen et al. (1992), together with the references therein. The major aspects of the applied numerical technique are summarized only briefly here for completeness.

The lattice-Boltzmann equation specifies the ensemble average behavior of a lattice gas in which discrete particles of unit mass move with unit speed along the edges of a regular lattice (McNamara and Zanetti 1989). Two- and three-dimensional (2-D, 3-D) projections of the four-dimensional Face-Centered-Hyper-Cubic (FCHC) lattice are commonly used for simulations of the Navier–Stokes equations (d'Humières et al. 1986). This FCHC lattice spans a four-dimensional space with 24 velocity directions $\mathbf{c}_i$ at each grid point. Figure 1 depicts the 2- and 3-D projections of this lattice with 9 and 18 velocity directions $\mathbf{c}_i$, respectively, and the weight factors m_i representing the multiplicity of the edges due to the projection. The lattice-Boltzmann scheme solves the lattice-Boltzmann equation directly without instantiating a discrete lattice gas, but operationally the procedure is very similar. A dimensionless mass density N_i is associated with each velocity direction $\mathbf{c}_i$ at each position $\mathbf{x}$ and time t. The evolution of the scheme involves two steps: a propagation step which shuffles all variables so that mass density N_i at position $\mathbf{x}$ moves to position $\mathbf{x}+\mathbf{c}_i$, and a collision step which redistributes the mass densities among the velocity directions at each grid point locally. Basically, the scheme solves the following set of coupled partial differential equations $\partial_t N_i + \mathbf{c}_i \cdot \nabla N_i = \Omega_i(\mathbf{N})$.

The so-called collision operator $\Omega_i(\mathbf{N})$ depends in a nonlinear way on all components of the mass density vector $\mathbf{N}$ and is constrained by the basic conservation laws of mass and momentum. The hydrodynamical modes, such as density ρ, pressure p, and velocity vector $\mathbf{u}$, are obtained from the mass densities N_i by simple summation rules. Analog to the velocity tensor $\mathbf{uu}$ and the rate of strain tensor $\nu(\nabla\mathbf{u} + (\nabla\mathbf{u})^T)$ that appear naturally in the lattice-Boltzmann scheme, a turbulent stress tensor $\boldsymbol{\tau}$ is introduced in our lattice-Boltzmann scheme to account for unresolvable velocity fluctuations at a scale smaller than the lattice spacing (see Eggels and Somers 1995). The standard Smagorinsky model (Smagorinsky 1963) without any further modifications is used to express this tensor in terms of known variables on the lattice.

Turbulent channel flow

Computational setup

To check the performance of our lattice-Boltzmann solver for simulations of turbulent flows, direct simulations with various grids are performed of the fully developed turbulent flow between two parallel plates. Heat transfer is incorporated by keeping the two plates at a constant but different temperature, the lower plate being warmer than the upper one. The influence of gravity is neglected, so buoyancy effects are not included. The two dimensionless parameters that describe the flow are the Reynolds number Re_* and the Prandtl number Pr, which are defined here as $\mathrm{Re}_* = u_* H/\nu$ and $\mathrm{Pr} = \nu/a$ with u_* the friction velocity based on the shear stress τ_w at the wall ($u_*^2 = \tau_w/\rho$), H half the channel height, ν the kinematic viscosity, and a the thermal diffusivity (ρ is the fluid density). In all our simulations, the values of Re_* and Pr are fixed at 120 and 0.71, respectively. The computational domain consists of two flat parallel plates of

Notation

a	thermal diffusivity
c_s	Smagorinsky coefficient
$\mathbf{c}_i$	velocity direction vector
C	ratio of overlap
D	impeller diameter
$\mathbf{f}$	force vector
H	half the channel height or total tank height
k	turbulent kinetic energy
m_i	weight factor for direction $\mathbf{c}_i$
N	rotational speed of impeller
N_i	mass density
$\mathbf{N}$	mass density vector
p	pressure
Pr	Prandtl number
r	radial coordinate
R	tank radius
Re	Reynolds number based on N, D, and ν
Re_*	Reynolds number based on u_*, H, and ν
t	time
t_{imp}	thickness of impeller blades
T	tank diameter
T^*	dimensionless temperature
T'	temperature fluctuation
T_c	temperature of cold wall
T_h	temperature of hot wall
T_m	mean temperature
T_o	impeller turn-around time
u_*	friction velocity based on wall shear stress
u_x, u_y, u_z	components of $\mathbf{u}$
u_x', u_y', u_z'	fluctuating components of $\mathbf{u}$
$\mathbf{u}$	velocity vector
U_{tip}	impeller tip speed
$\mathbf{U}_f$	local fluid velocity vector
$\mathbf{U}_i$	local impeller velocity vector
w	width of impeller blades
$\mathbf{x}$	position vector
$y^+ = yu_*/\nu$	dimensionless distance from the wall

Greek

α	relaxation factor
$\Delta^+ = \Delta u_*/\nu$	dimensionless grid spacing
Δt	time-step
$\eta^+ = \eta u_*/\nu$	dimensionless Kolmogorov length scale
ν	kinematic viscosity
ρ	density
ρ_T	correlation coefficient
τ	subgrid-scale turbulent stress tensor
τ_w	wall shear stress
Ω_i	mass density collision operator

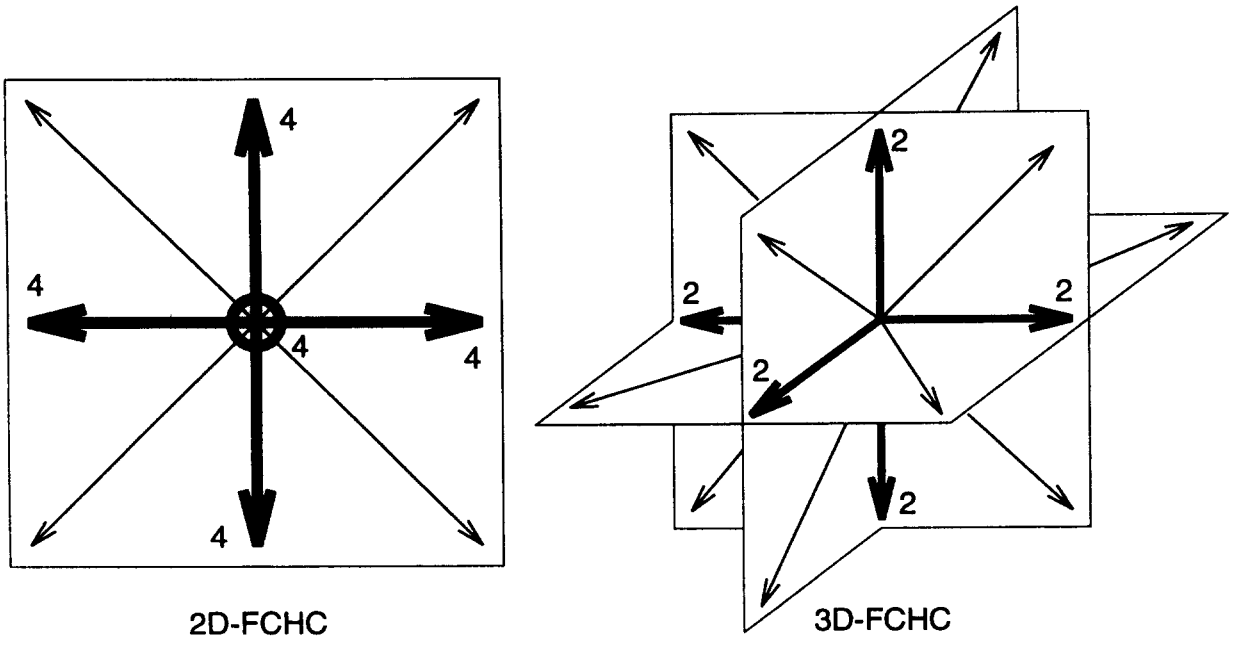

Figure 1 The two- and three-dimensional projections of the Face-Centered-Hyper-Cubic lattice correspond to an ordinary square and cubic lattice with 9 and 18 velocity directions $\mathbf{c}_i$ respectively. The numbers along the edges indicate their multiplicities m_i, which, according to the original four-dimensional lattice, satisfy $\Sigma_i m_i = 24$

size $6H \times 3H$ separated at a distance of $2H$ with periodic boundary conditions in the streamwise and spanwise directions and no-slip velocity and Dirichlet temperature conditions on both walls. In terms of the viscous length scale ν/u_*, the size of the domain is $720 \times 360 \times 240$ in the streamwise, spanwise, and vertical directions. In comparison to previous direct simulations reported in the literature (Kim et al. 1987; Lyons et al. 1991), the size of the present computational domain is limited and the imposed periodicity may affect the flow statistics. On the other hand, the two-point correlation coefficients reported by Kim et al. are small (< 0.10) at separation distances of half the present channel length, which indicates that the computational domain employed is not yet too small. Three direct simulations are performed for which all conditions except the grid spacing are kept constant. The uniform (for a discussion on the use of uniform grids, see Eggels and Somers 1995) grid spacing Δ^+ in terms of ν/u_* is reduced from 6.0 in the coarsest simulation via 3.0 to 2.4 in the finest. The number of grid points thus increases from $120 \times 60 \times 40 = 2.88 \cdot 10^5$ up to $300 \times 150 \times 100 = 4.5 \cdot 10^6$. At the present Reynolds number, the Kolmogorov length scale η^+, scaled with ν/u_*, is estimated to be about 2 (see Kim et al.). Following the criteria suggested by Grötzbach (1983), in all except the coarsest simulation a sufficiently fine grid is applied.

Results

The flow statistics obtained from the direct simulations by spatial averaging in the homogeneous streamwise and spanwise directions and by time-averaging over six time-scales H/u_* are compared for the different grids and with the numerical results reported by Kim et al. (1987). Although the Reynolds number in the direct simulation by Kim et al. is somewhat larger ($\mathrm{Re}_* = 180$) than in the present study, the statistics in the near-wall region should be similar when scaled on inner scales. The mean velocity profile is shown in Figure 2 as a function of the distance from the wall in wall units. Up to $y^+ = 20$, the results of the finest grid simulations closely match those reported by Kim et al. Beyond $y^+ = 20$, the differences in Reynolds number appear as deviations

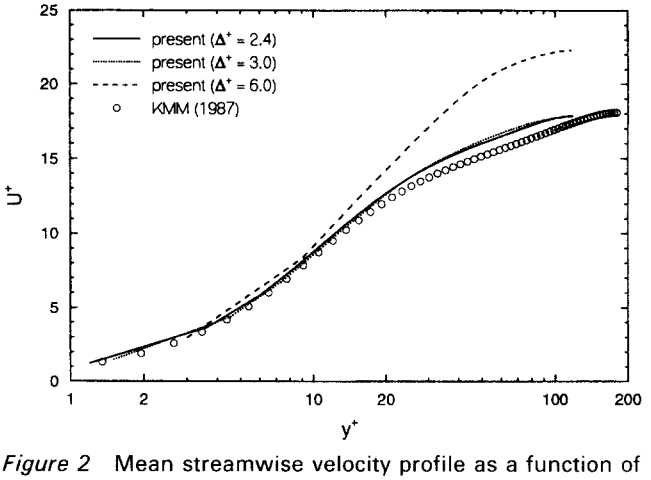

Figure 2 Mean streamwise velocity profile as a function of the distance from the wall in wall units

of the mean velocity profiles (no log-law with "universal" coefficients yet at $\mathrm{Re}_* = 120$). The effect of grid refinement from $\Delta^+ = 3.0$ to $\Delta^+ = 2.4$ is negligibly small. The simulation with $\Delta^+ = 6.0$ obviously provides inaccurate results because of the too coarse grid due to which the steep gradients near the walls are not properly resolved. The root-mean-square (rms) velocities versus y/H are plotted in Figure 3. Grid refinement from $\Delta^+ = 3.0$ to 2.4 again only has a limited influence on the statistics, except for the streamwise rms velocity in the core region of the flow ($y/H > 0.4$). In Figure 4, the rms velocities are scaled with the local mean streamwise velocity and plotted in the near-wall region only. According to Rai and Moin (1991), this way of presenting the rms velocities gives a good impression of the accuracy of the numerical scheme. Very close to the wall, a constant value of about 0.36 should be found for the streamwise velocity fluctuations. From the present simulations, we obtain

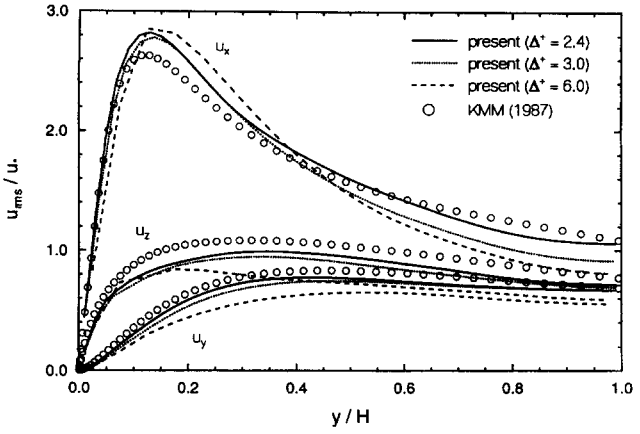

Figure 3 Root-mean-square (rms) velocities as a function of the distance from the wall; the streamwise, normal-to-the-wall and spanwise components are denoted by x, y, and z, respectively

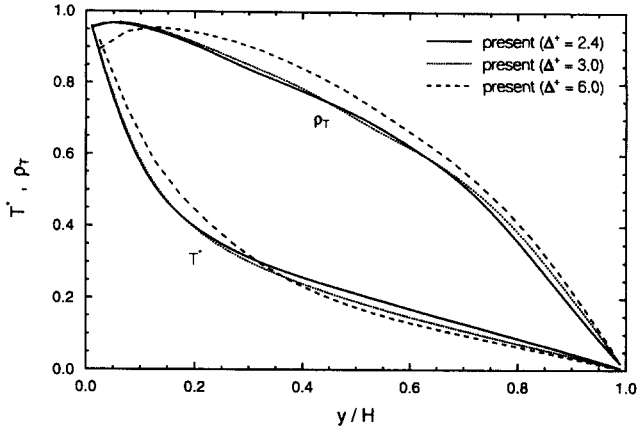

Figure 5 Mean temperature distribution T^* and correlation coefficient ρ_T across the channel from the hot wall up to the centerline

0.336 ($\Delta^+ = 3.0$) and 0.354 ($\Delta^+ = 2.4$), which is in close agreement with the results reported by Kim et al. and Rai and Moin. The decrease of the streamwise velocity fluctuations when moving away from the wall is in excellent agreement with Kim et al. Also the vertical velocity fluctuations agree well, but the spanwise fluctuations are somewhat lower in our simulation, most pronounced, but not limited to, the vicinity of the wall. The observation that the spanwise fluctuations are also too low in the interior of the channel suggests that the limited spanwise extent of the channel may have had an effect on spanwise motions. Figure 5 shows the dimensionless temperature distribution $T^* = (2T_m - T_h - T_c)/(T_h - T_c)$ (T_h and T_c denote the temperature of the hot [lower] wall and the cold [upper] wall, respectively) for the hot wall together with the correlation coefficient ρ_T. It is defined here as:

$$\rho_T = -\frac{\overline{u'_x T'}}{u_{x,\mathrm{rms}} T_{\mathrm{rms}}}$$

and expresses the correlation between the streamwise velocity fluctuations u'_x and the temperature fluctuations T'. Near the hot wall, ρ_T approaches unity, which indicates that locally high temperatures are found in low-speed regions; whereas, locally low temperatures are found in regions with high streamwise velocity. This picture is consistent with the concept of ejections and sweeps transporting relatively warm low-speed fluid away from the wall and relatively cold high-speed fluid from the interior towards the wall. Near the cold wall, the overall picture is just opposite with ρ_T now approaching -1. Here the near-wall low-speed fluid is colder than the ambient fluid; whereas, the high-speed fluid coming in from the interior is relatively warm.

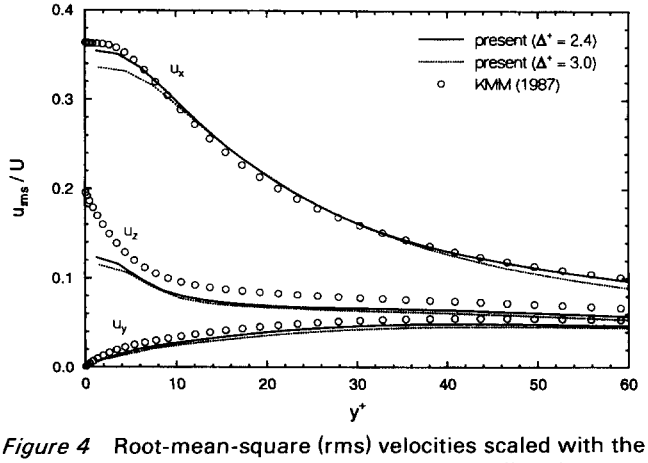

Figure 4 Root-mean-square (rms) velocities scaled with the local mean streamwise velocity in the near-wall region

Baffled stirred tank reactor flow

Impeller modeling

One of the flow problems frequently encountered in the (petro)chemical industry is the flow in a stirred vessel, mechanically driven by an impeller. Information on the (time-dependent) flow field in the vessel is important for an optimal design of the reactor, because the efficiency of such systems depends, among other things, on the flow generated by the impeller and, therefore, on the shape of the impeller, its position in the reactor, its rotational speed (in general, the operational conditions), and the vessel geometry. Numerical simulations of such reactor systems are helpful to investigate the effects of different impeller shapes, vessel geometries, and operational conditions in order to provide designers with detailed information. In contrast to computations that directly solve the time-averaged Navier-Stokes equations using conventional turbulence models, the unsteady and quasi-periodic behavior of the flow in such configurations can be accounted for in a natural way using LES. Furthermore, LES data can increase our insight and understanding of the dynamical behavior of such systems. Therefore, if it is possible to model the impact of a mechanical impeller via a spatially and/or temporally varying force field $\mathbf{f}(\mathbf{x}, t)$ on the momentum equations of the fluid, then it is possible to simulate flows in stirred vessels with our lattice-Boltzmann solver, because it can easily account for such spatially and/or temporally varying force fields. A first such model as that which has recently been implemented in our solver, is one in which the force vector $\mathbf{f}(\mathbf{x}, t)$ depends linearly on the difference between the local fluid velocity vector $\mathbf{U}_f$ and the local velocity vector of the impeller $\mathbf{U}_i$:

$$\mathbf{f}(\mathbf{x}, t) = \alpha C(\mathbf{x}, t)\rho(\mathbf{U}_i(\mathbf{x}, t) - \mathbf{U}_f(\mathbf{x}, t))/\Delta t$$

The idea of this model is to force the fluid velocity vector *locally* to the velocity vector of the impeller, preferably within one (or a few) time-steps Δt, as if the impeller were actually

present at that location. The relaxation factor α controls the speed at which the fluid velocity responds to the impeller velocity and should be somewhat smaller than unity. With α equal to unity, the fluid velocity is forced instantaneously to the local impeller velocity. Such a rapid response, however, may give rise to instabilities or oscillations. On the other hand, we do not want to fix α at a too small value, because we want the fluid to respond rapidly to the motion of the impeller. Therefore, the use of a value for α that is somewhat smaller than unity is recommended. In the present simulations, we imposed, rather arbitrarily, $\alpha = 0.95$. Further investigations focusing on the influence of different values for α are certainly required. The coefficient $C(\mathbf{x},t)$ in the model varies between 0 and 1 and controls where, when, and to what extent the force field actually acts on the momentum equations of the fluid. It should be interpreted as the ratio of overlap of a grid volume with the volume of the impeller. The local value of this coefficient as a function of time, therefore, depends on the shape of the impeller and its position and orientation in the computational domain. Obviously, its value has to be evaluated every time-step for a selected range of grid points.

Configuration

To check the performance of this model accounting for the presence of a mechanical impeller, the turbulent flow in a standard configuration consisting of a vessel with four baffles and a 6-blade disc turbine is simulated. This configuration has been studied extensively in the past, both experimentally and numerically (see, e.g., Ranade and Joshi 1990a, 1990b and the references therein), and should, therefore, be regarded as a suitable test case. The standard Smagorinsky model (Smagorinsky 1963) without further modifications and with $c_s = 0.10$ is applied in our LES for modeling the subgrid-scale stresses. The vessel configuration together with a sketch of the impeller shape in front and top view are shown in Figure 6. In the simulations, the shaft on which the impeller is mounted is neglected. At the side wall and the bottom of the vessel, no-slip velocity conditions are applied; whereas, at the top of the vessel, a flat free surface is effectuated through the use of free-slip velocity conditions. The Reynolds number defined as $\mathrm{Re} = ND^2/\nu$ with N the rotational speed of the impeller equal to 250 [rpm] (the impeller turn-around time $T_o = 0.24$ [s]) and $D = 160$ [mm] the impeller diameter, is equal to $1.07 \cdot 10^5$. This value is sufficiently large to assume that the turbulence is fully developed.

Temporal monitoring of the velocity and the energy levels in a subsection of the vessel revealed that at least $30T_o$ should be simulated when starting from zero velocity fields before the flow reaches a quasi-steady state. This is illustrated in Figure 7, where the evolution of the resolved and subgrid-scale turbulent kinetic energy, averaged over the upper half part of the reactor, is plotted as a function of time for one of those simulations. Once a quasi-steady state has been reached, low-frequency variations with a time-scale of the order of $10\text{–}20T_o$ are observed, which indicate that the sampling interval for collection of the flow statistics should be sufficiently long to capture these low-frequency variations. Such low-frequency variations have also been observed experimentally.

The results of two BSTR simulations are reported in the next section. These two simulations are largely the same, except for a few parameter settings. The first parameter that is changed is the spatial resolution. Simulation A is performed using a uniform grid size of 4 mm; hence, with a spatial resolution of $120^3 = 1.73 \cdot 10^6$ grid points. In simulation B, the grid spacing is halved to 2 mm, which brings the number of grid points at $240^3 = 13.8 \cdot 10^6$. With the refinement of the grid, the thickness t_{imp} of the

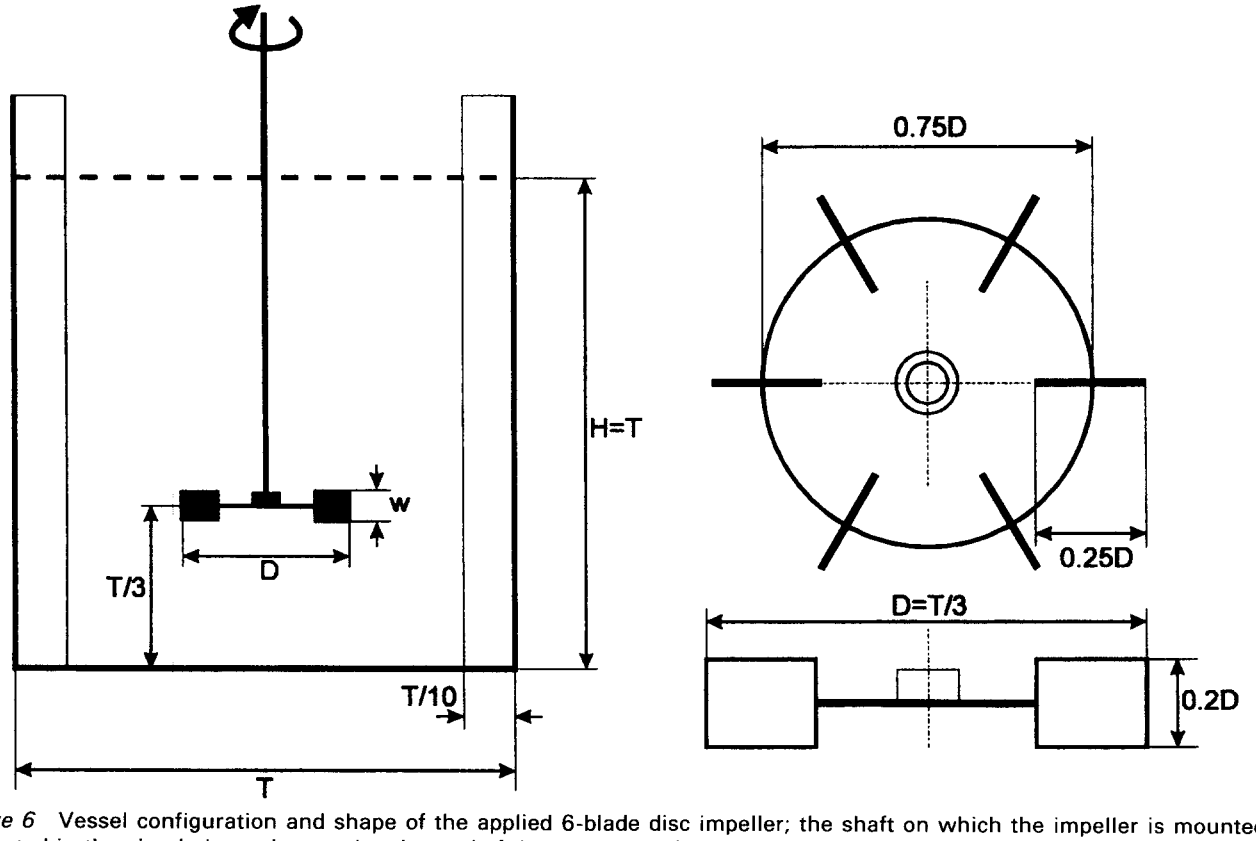

Figure 6 Vessel configuration and shape of the applied 6-blade disc impeller; the shaft on which the impeller is mounted is neglected in the simulations; the rotational speed of the impeller is fixed at 250 rpm

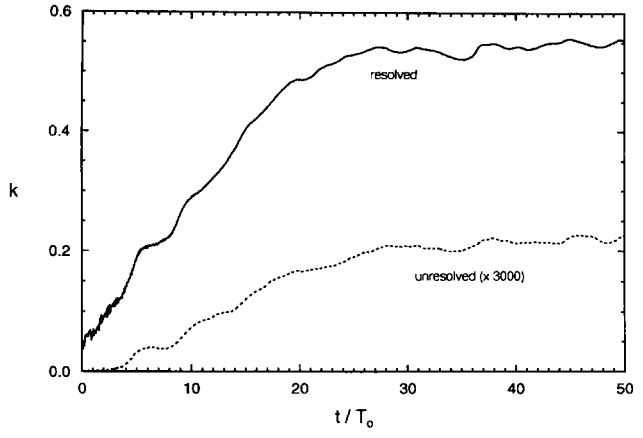

Figure 7 Evolution of the resolved and subgrid-scale turbulent kinetic energy as a function of time; for scaling purposes, the subgrid-scale energy is multiplied by 3000; the kinetic energy is scaled with U_{tip}^2; note that in this upper part of the reactor, the subgrid-scale energy is extremely small compared to the resolved kinetic energy

impeller blades is also reduced from $t_{imp} = 4.0$ mm (0.125 w, with w the width of the impeller blades equal to $0.2D$) for simulation A to $t_{imp} = 2.2$ mm (0.069 w) for simulation B. From earlier experiments, it is known that the thickness of the impeller blades can have a substantial effect, especially on the fluctuation levels of the velocity components (H. R. E. van Maanen personal communication, Shell Research, Amsterdam). To match closely the thickness of the blades used in the experiment (0.105 w for the measurements reported by Bakker 1995), the blade thickness in the simulations is reduced with decreasing grid spacing. (A blade thickness smaller than the grid spacing cannot be accounted for properly in the present impeller model. Effectively, the model will mimic a more or less porous impeller blade in such situations. Therefore, the blade thickness must be rather large in simulation A to remain of the order of the grid spacing.) As we will see later, grid refinement and the reduced thickness of the impeller blades, indeed, have a reasonable influence on the flow statistics near the impeller. The second parameter that is changed is the length of the sampling interval. In simulation A, the length of the sampling interval is $30T_o$, in B it is $8T_o$. In B, it is shorter only to keep the required CPU time within limits. The consequence, however, is that the statistics are influenced by the limited length of the interval, which is apparent from the fact that the statistics are not yet symmetric with respect to the symmetry axis of the configuration (statistical noise). To limit the CPU time of simulation B further, it is started from a velocity field stored during simulation A, being interpolated to the proper spatial resolution. Simulation A, on the other hand, is started from a zero velocity held.

Finally, a few words about the computer demands for this kind of simulations. All simulations are performed running in parallel mode on the IBM/SP2. Using the 4.0 mm grid with 120^3 grid points, the maximal memory demand during "on-the-fly" averaging of the statistics is about 550 Mb. The CPU time per T_o (750 time-steps) is about 1 hour on 8 nodes of the SP/2 without averaging and 1.6 hours with averaging. (The "on-the-fly" averaging procedure to collect the flow statistics requires additional work to be done and data exchange (communication) between the various processors. This overhead can be significant, especially when the sample frequency is high.) Therefore, a typical simulation running for $20T_o$ to develop and $40T_o$ to collect the statistics takes about 85 hours. On the 2.0 mm grid with 240^3 grid points, the maximal memory demand during the "on-the-fly" averaging stage is 2200 Mb. This simulation required 7 CPU hours per T_o (1500 steps) on 16 nodes IBM/SP2 in single precision (8.8 hours during averaging with the sample frequency set to every fifth time-step). Obviously, these kinds of simulations can easily run for hundreds of CPU hours and, therefore, require careful timing and preparation.

Results

The overall flow pattern in the reactor is illustrated in Figures 8–11 showing instantaneous and time-averaged vector fields in a vertical midplane of the reactor and in a horizontal plane just above the impeller. These plots are obtained from simulation A and shown on the same resolution as that applied in the simulation. The impeller located at $z = 0$ is not visible directly but only indirectly through the flow field. In Figure 9, small trailing vortices are visible at the "inside" of the six impeller blades. In the mean, evidently, they vanish. Unless stated otherwise, all velocities presented further on are scaled with the tip speed of the impeller, defined as $U_{tip} = \pi D/T_o$, and shown for a plane in the middle between two baffles. In each of the following figures, the upper plot shows the data obtained from simulation A, and the lower plot shows those from fine-grid simulation B. The numerical data are represented by the lines, and the corresponding experimental data, by markers.

Figures 12 and 13 show the mean and rms velocities of the radial component in the impeller stream for various radial positions $r/R = 2r/T$ from the impeller centerline. The flow generated by the disc impeller closely resembles a jet in the impeller stream, characterized by a decreasing mean radial velocity on the centerline ($2z/w = 0$) and an increasing width of the jet downstream as a result of entrainment. Agreement of the numerical data with the experimental ones of Wu and Patterson (1989) is acceptable, in particular for simulation B. In simulation A, the maximal radial velocity is found away from the impeller, in contrast to the experiment and simulation B. This might be due to the fact that the impeller blades in this simulation are thicker than in the experiment and in simulation B. A similar behavior is also found in experiments of Ranade and Joshi (1990a, p. 23), although it is not clear from their paper under what conditions. The rms velocity shown in Figure 13 are somewhat larger near near the impeller in simulation B compared to A (this effect is stronger for the tangential and axial components, not shown here). The reason for this is that the impeller blade thickness in the fine grid simulation is smaller than in the coarse grid simulation. As already mentioned before, we know from experiments that this effect, indeed, enhances the velocity fluctuations, at least near the impeller. Away from the impeller, say for $r/R > 0.6$, the deviations between the rms velocity profiles from the two simulations rapidly diminish.

Figures 14 and 15 show the mean and rms velocity profiles along a vertical traverse running from the bottom of the reactor ($z/D = -1$) up to the free surface ($z/D = 2$) at the radial position $r/R = 0.340$. Both the radial and axial components are shown and compared with the experimental data by Bakker (1995). For the mean flow and the rms, two lines are shown simultaneously for the simulations taken from opposite sides of the symmetry axis of the configuration. The deviations between the two lines illustrate the asymmetry of the statistics because of the limited length of the sampling interval. The overall agreement between simulations and experiments is good. The axial rms velocity near the impeller is strongly affected by the increase of the resolution and related reduction of the blade thickness. Some specific details of the profiles in the vicinity of the impeller, however, are not yet predicted in complete agreement with the experiments; e.g., the local minimum of the mean axial velocity around $z/D = -0.10$ and the asymmetry of the axial rms peaks. It is not inconceivable, in this respect, that subtle

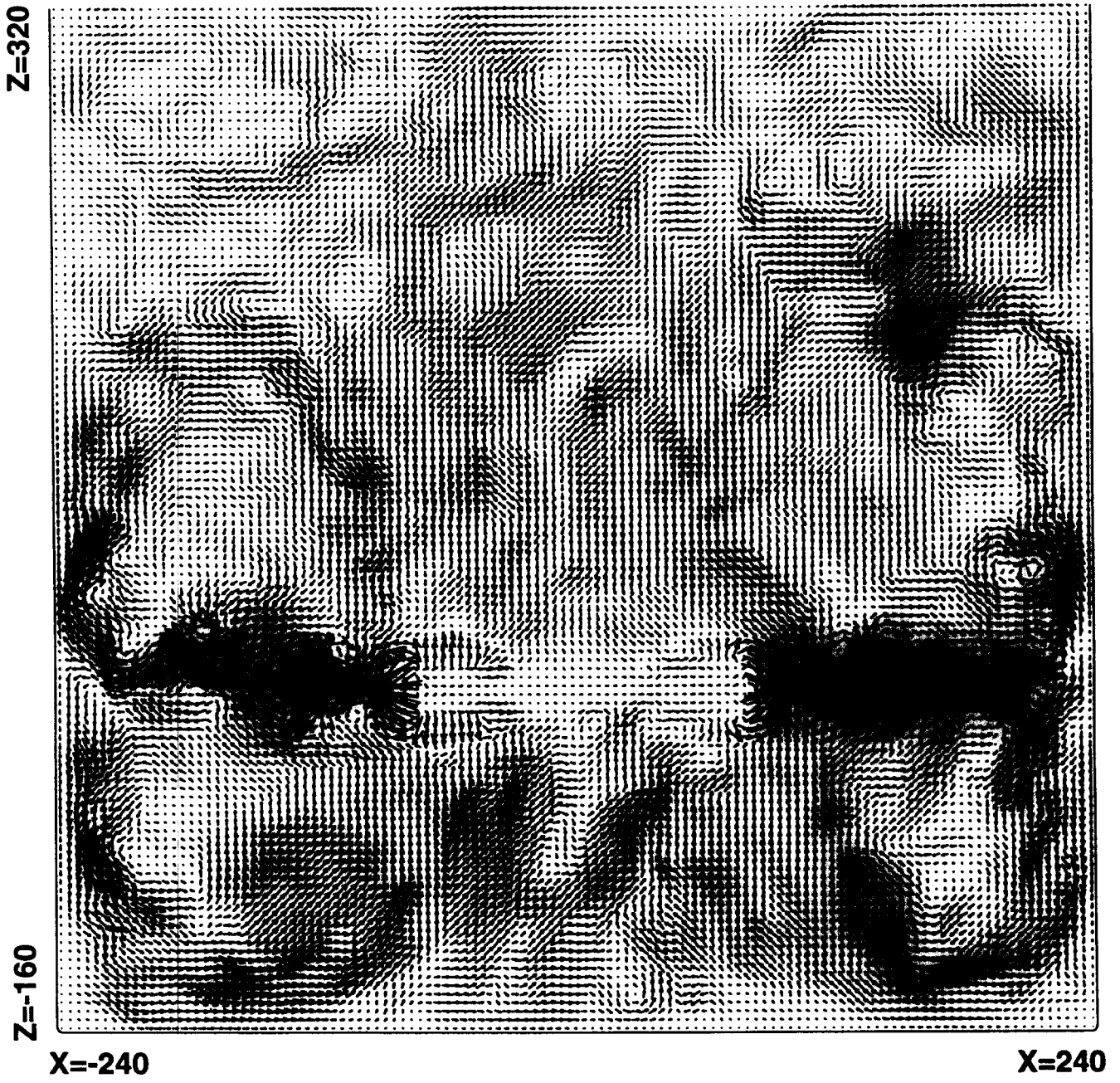

Figure 8 Instantaneous vector field of the turbulent flow in a vertical midplane of the stirred reactor tank; the impeller located at $z=0$ is only indirectly visible through the flow field because its presence is modeled in terms of a varying force field; the data are taken from simulation A; the resolution shown in this plot is the same as applied in the simulation

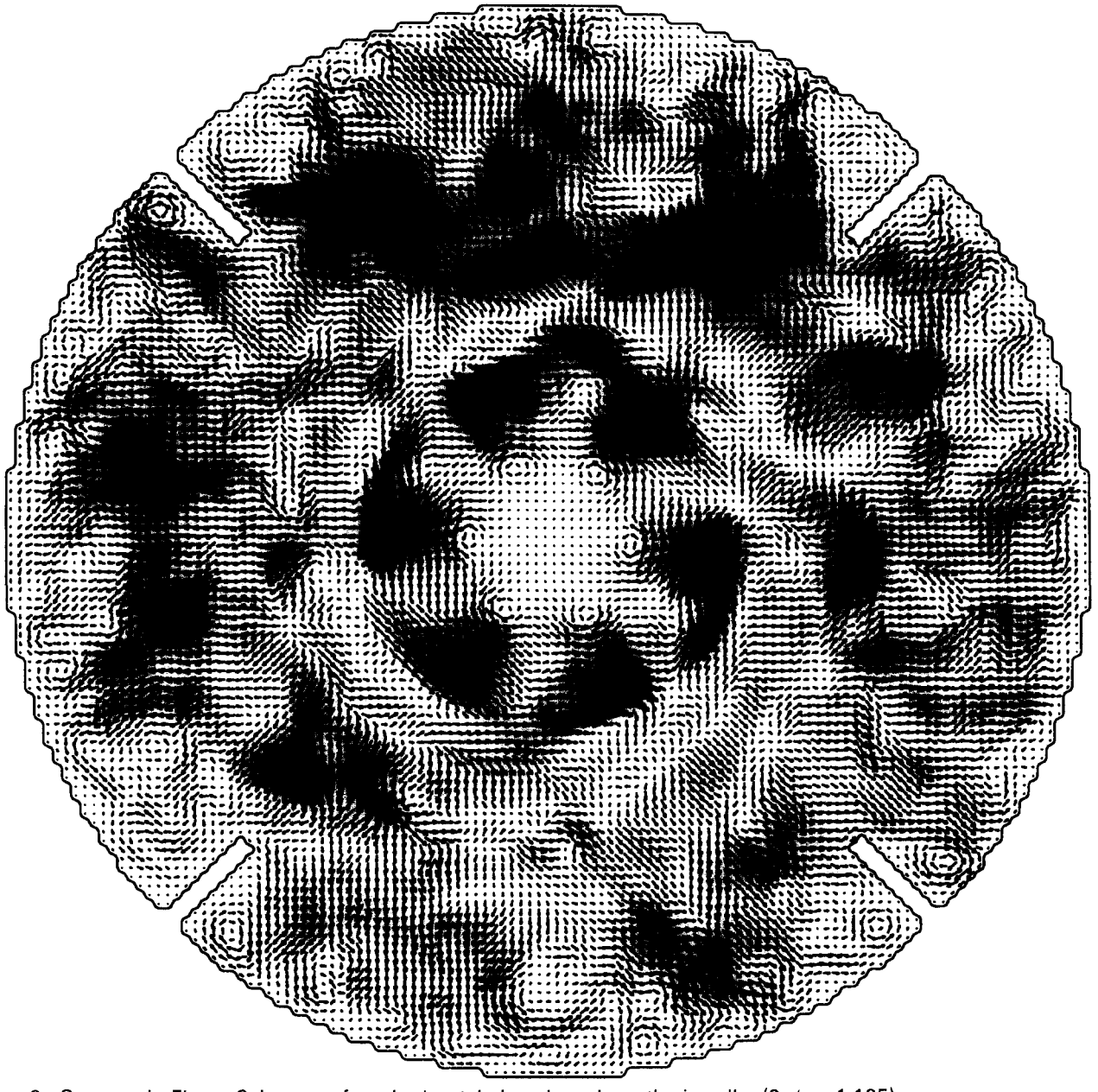

Figure 9 Same as in Figure 8, but now for a horizontal plane just above the impeller ($2z/w = 1.125$)

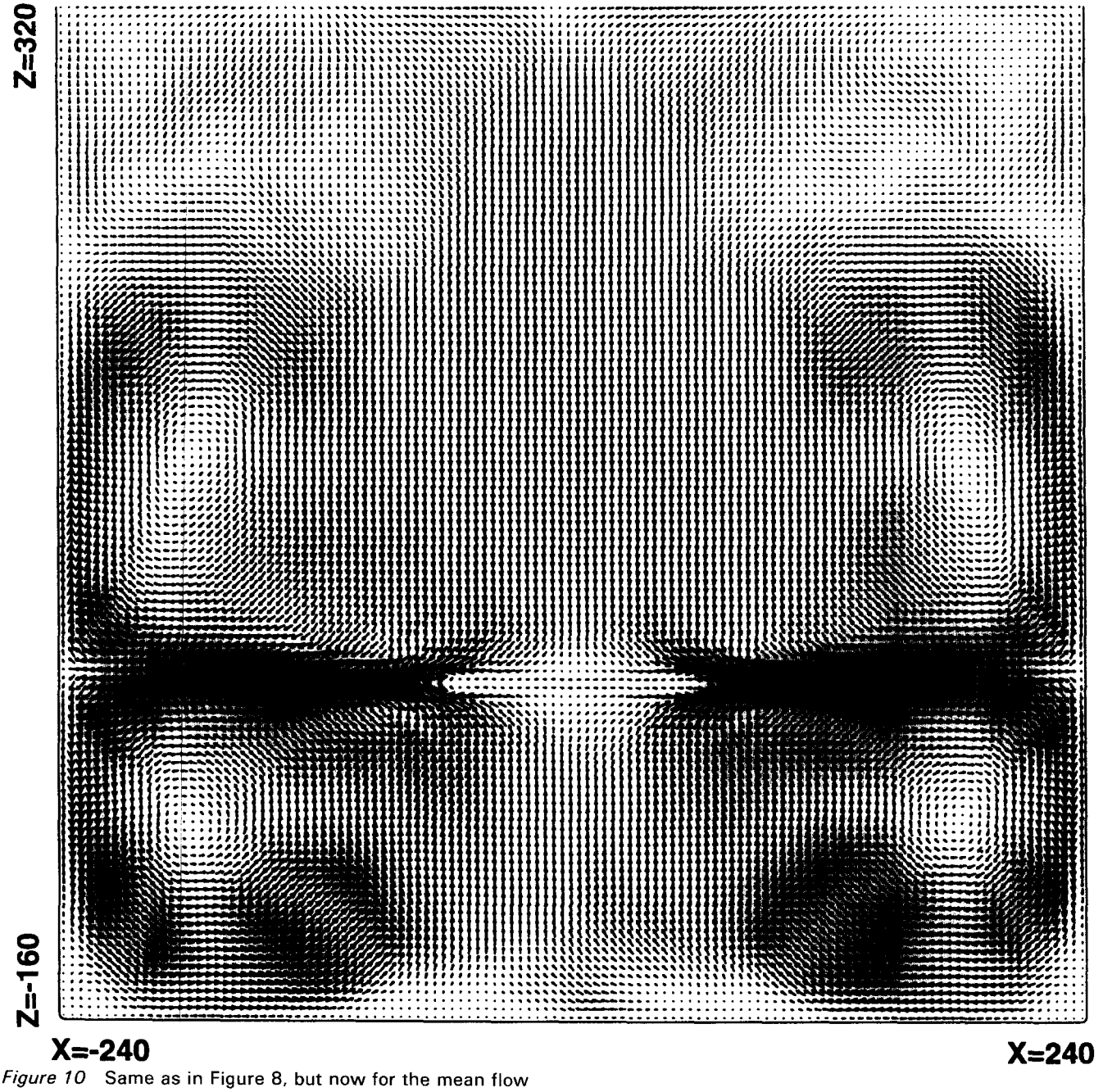

Figure 10 Same as in Figure 8, but now for the mean flow

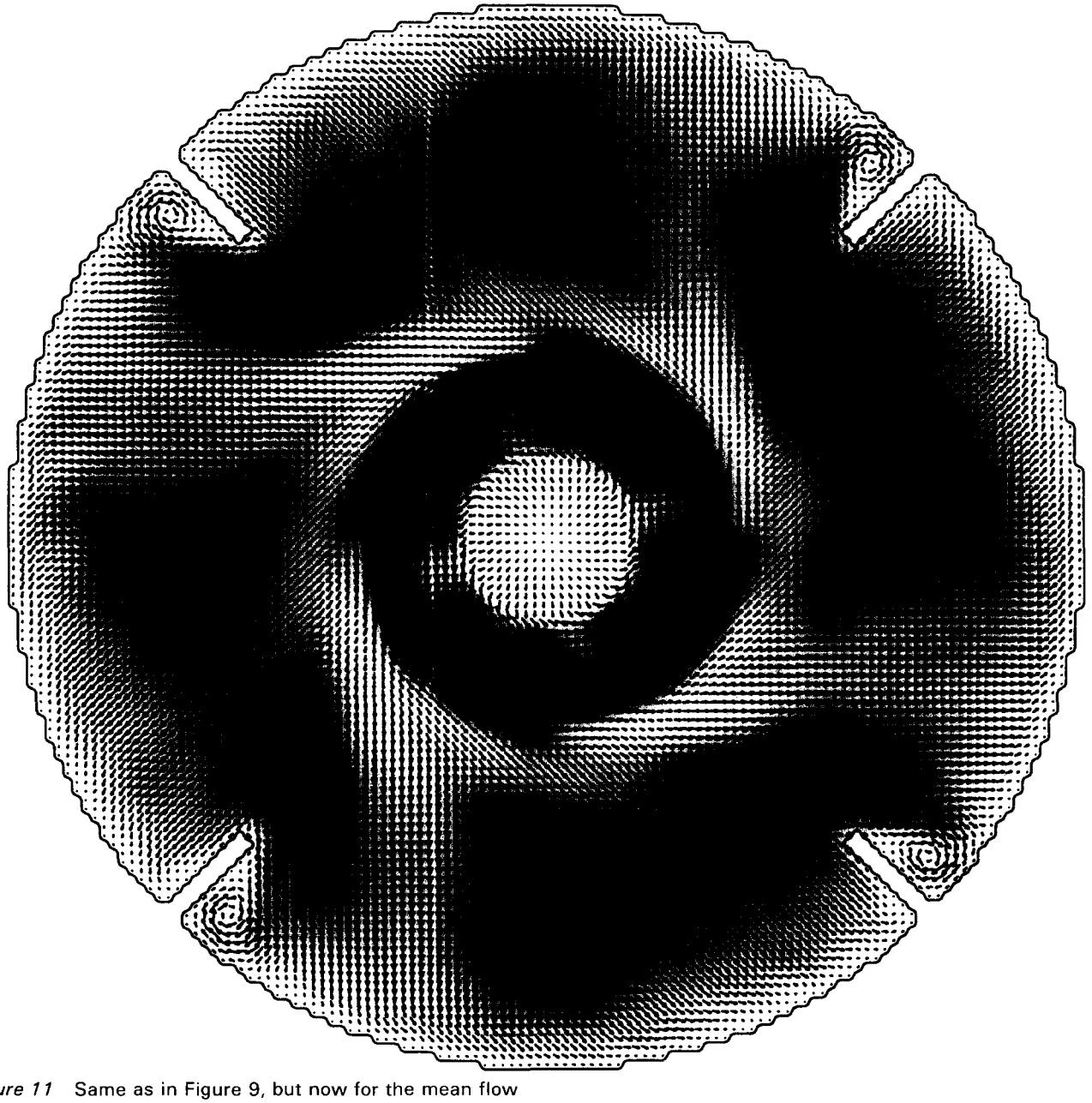

Figure 11 Same as in Figure 9, but now for the mean flow

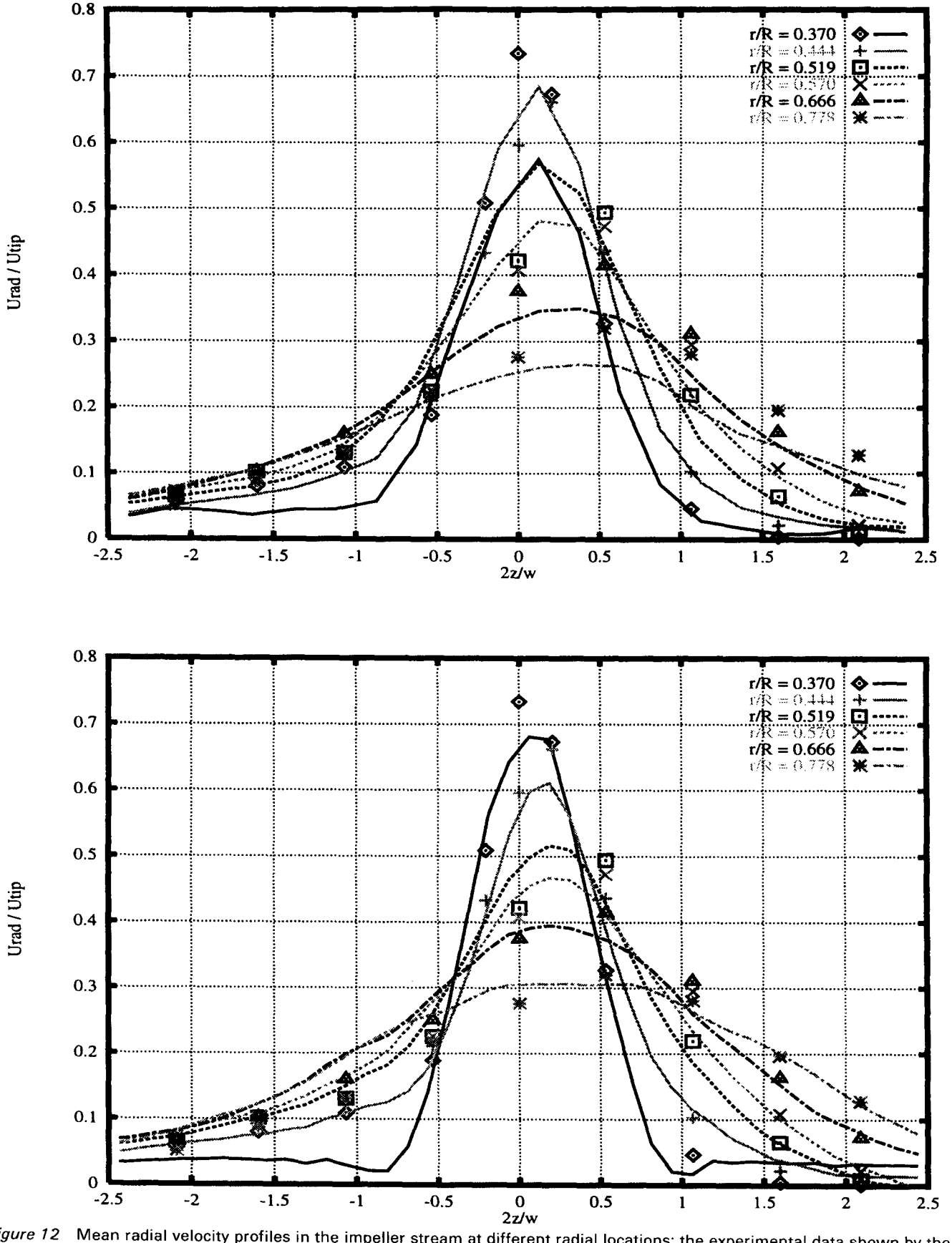

Figure 12 Mean radial velocity profiles in the impeller stream at different radial locations; the experimental data shown by the markers are taken from Wu and Patterson (1989)

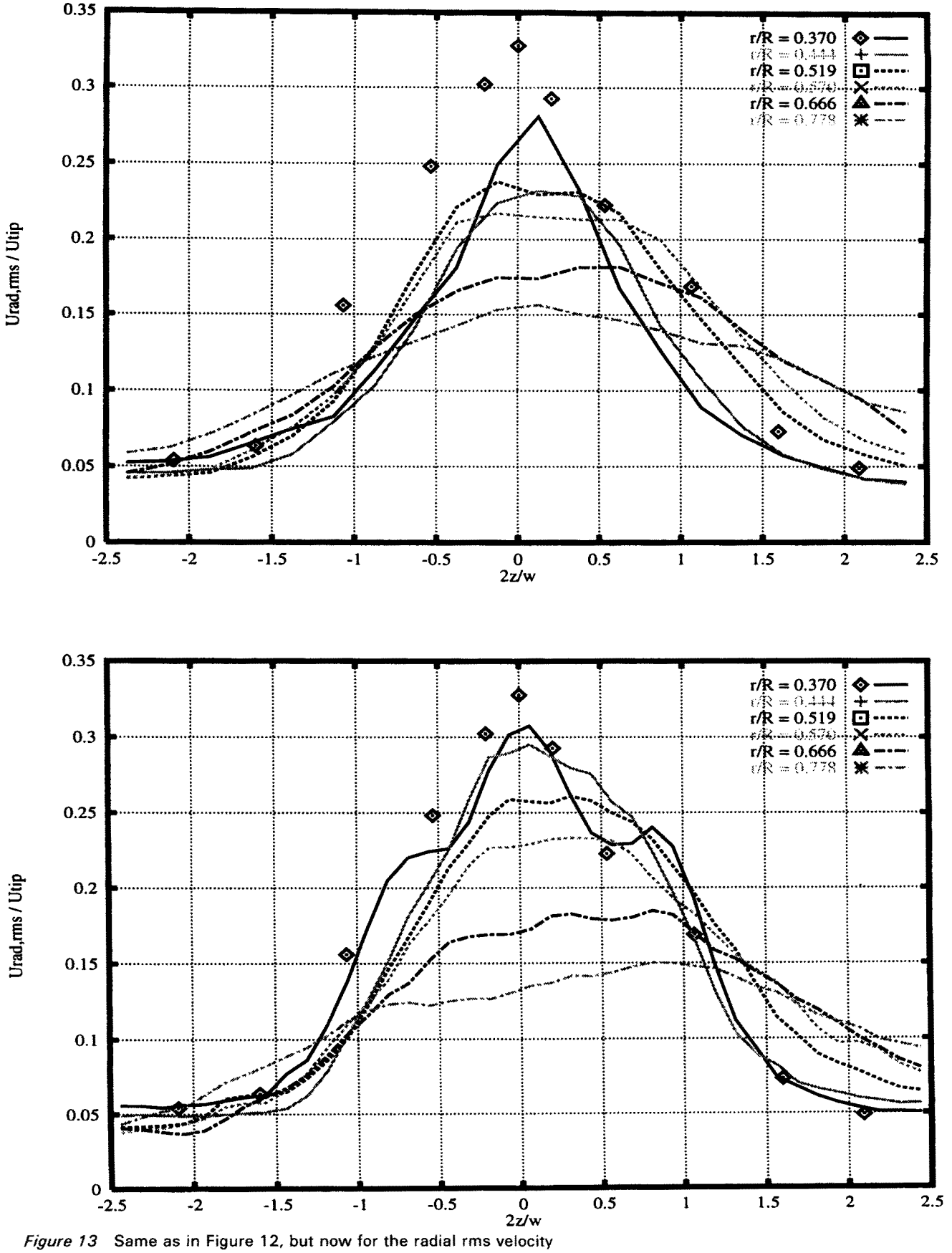

Figure 13 Same as in Figure 12, but now for the radial rms velocity

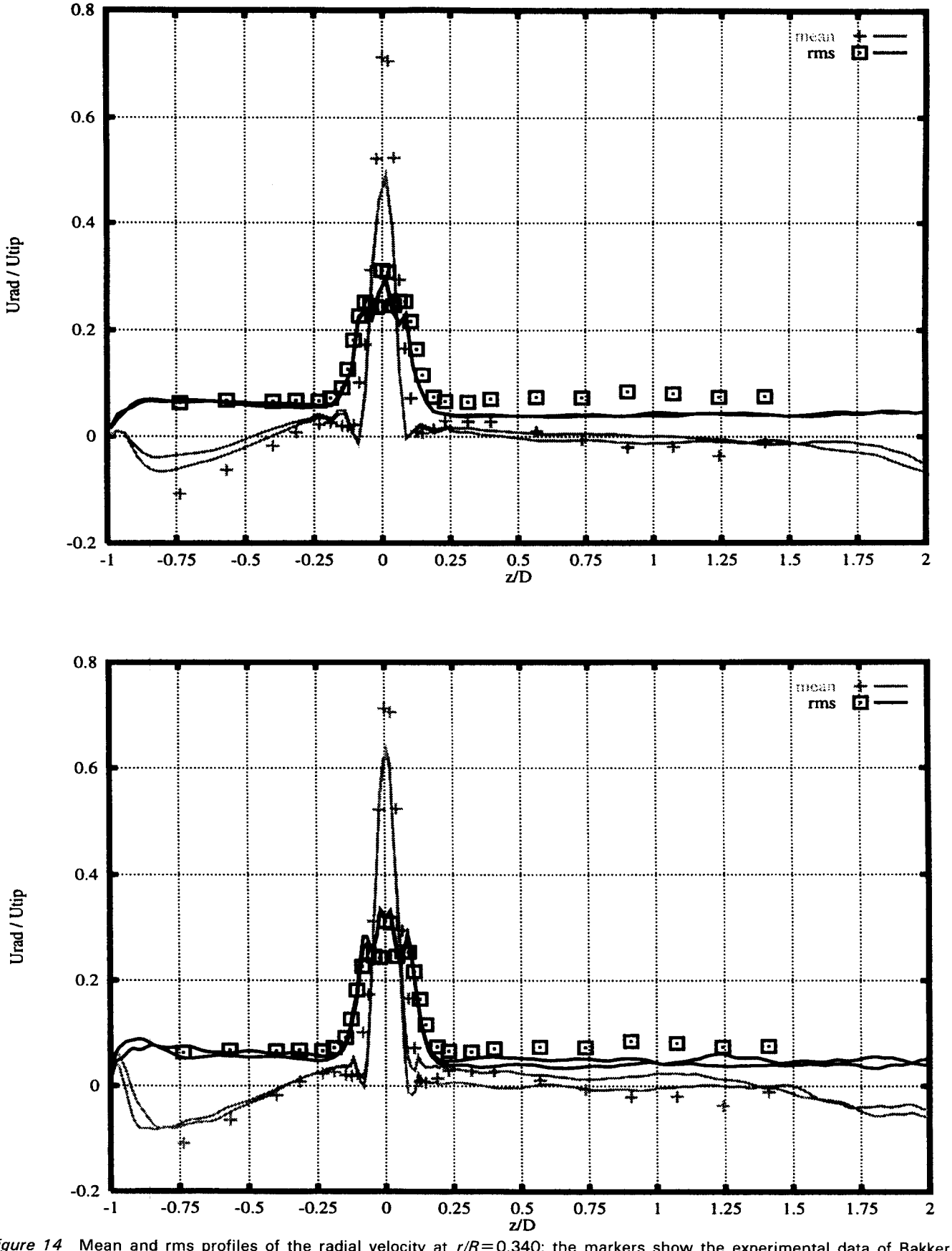

Figure 14 Mean and rms profiles of the radial velocity at $r/R=0.340$; the markers show the experimental data of Bakker (1995)

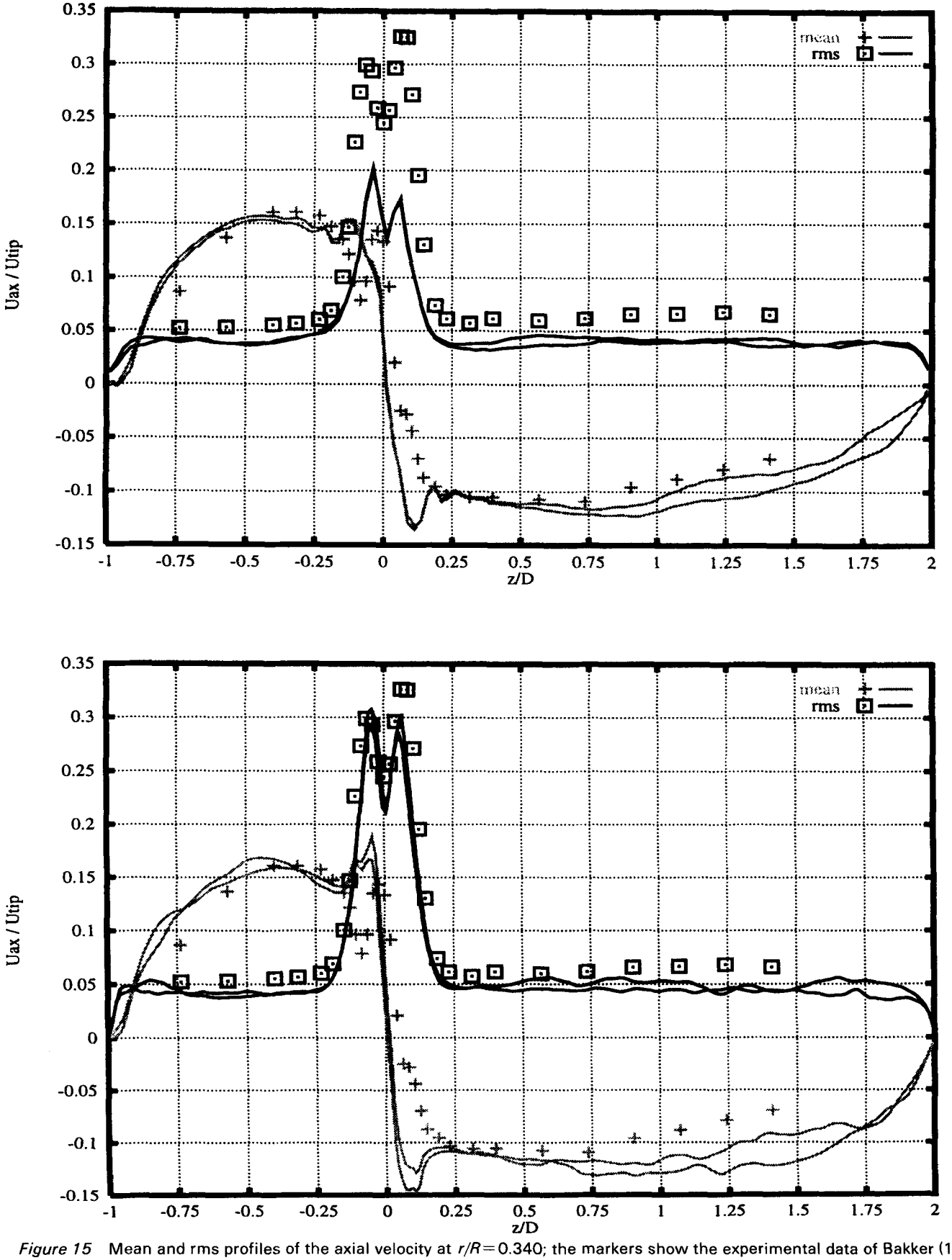

Figure 15 Mean and rms profiles of the axial velocity at $r/R=0.340$; the markers show the experimental data of Bakker (1995)

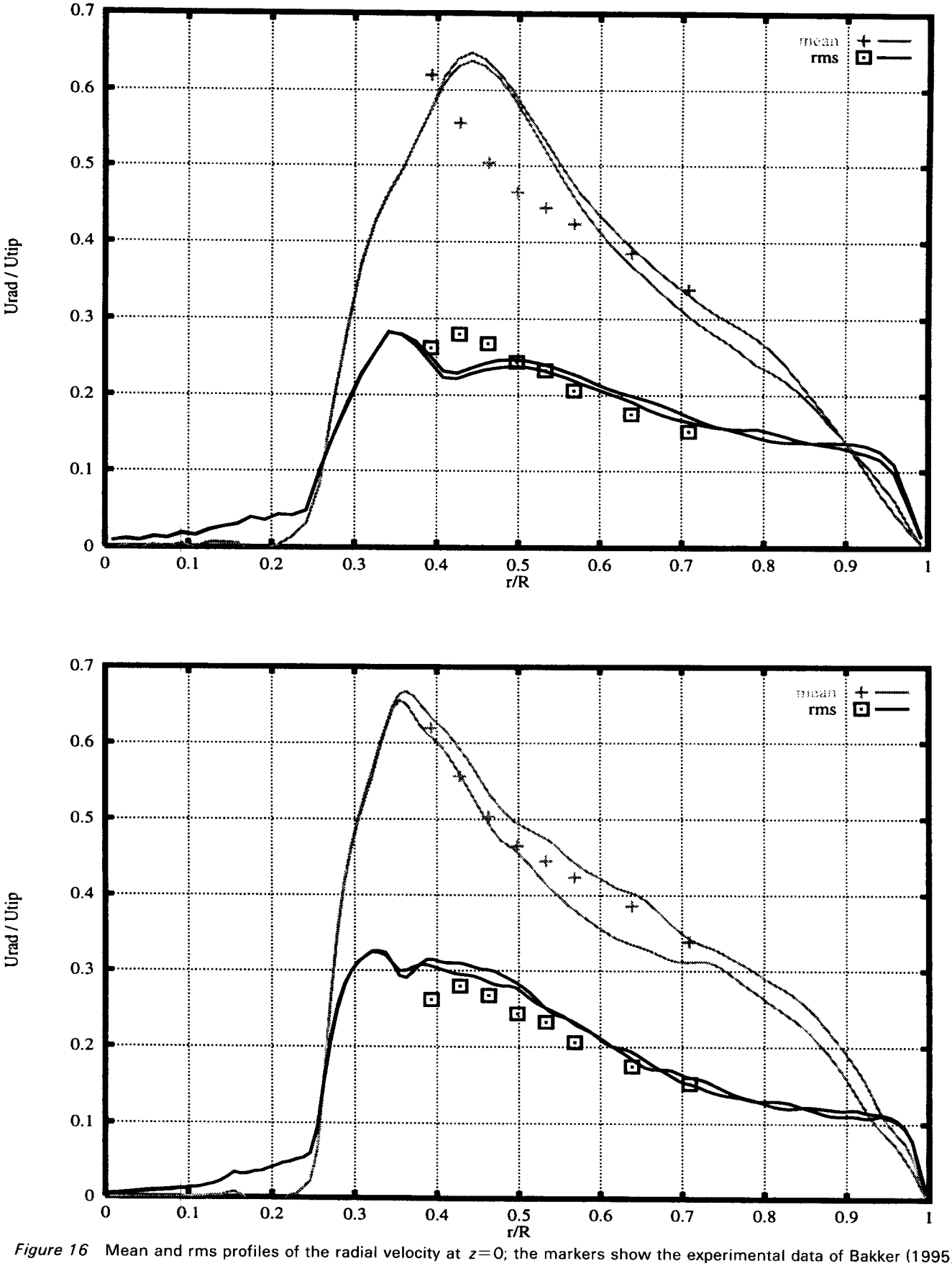

Figure 16 Mean and rms profiles of the radial velocity at $z=0$; the markers show the experimental data of Bakker (1995)

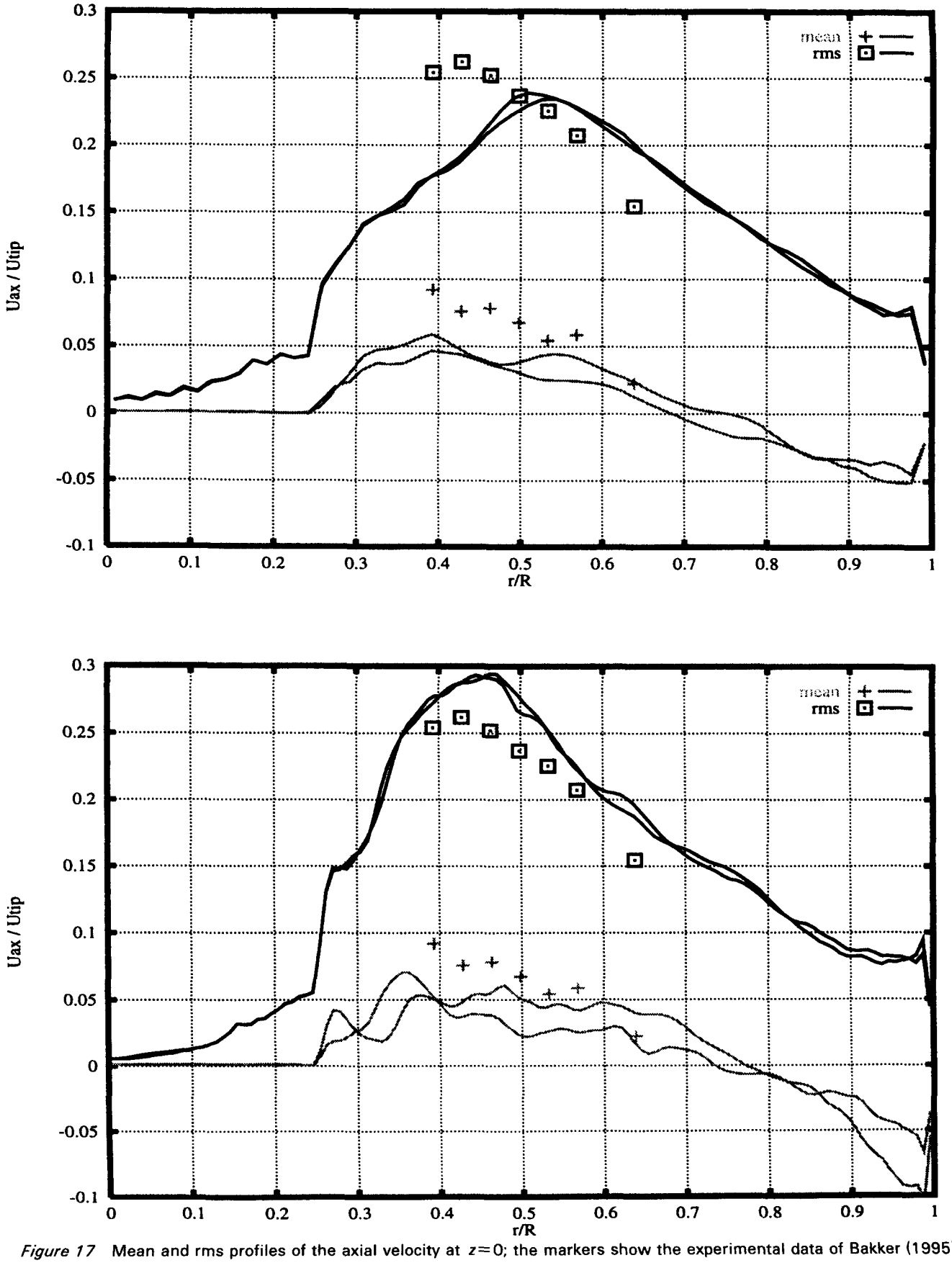

Figure 17 Mean and rms profiles of the axial velocity at $z=0$; the markers show the experimental data of Bakker (1995)

impeller blade details, such as rounded tip corners or minor imperfections that are not accounted for in the present simulations, play an important role in the establishment of the fluctuation levels this close to the impeller.

Finally, in Figures 16 and 17, the radial and axial mean and rms velocity profiles are shown along a horizontal traverse through the impeller midplane ($z = 0$). The jet-like behavior of the flow in the impeller stream is evident. The asymmetric global circulation in the reactor due to the fact that the impeller is placed at $z = 1/3\nu H$ together with the free surface at the top in contrast to the solid wall at the bottom, is apparent from the mean axial velocity profile in Figure 17. Here, we clearly see downflow near the wall in the impeller midplane as a result of the impeller jet being deflected upward.

Conclusions

The direct numerical simulation results presented in this paper show that the lattice-Boltzmann scheme can be used successfully to simulate turbulent flows. In our first attempt to simulate the turbulent flow in a baffled stirred tank reactor by means of large-eddy simulation, the concept of modeling the impact of a mechanical impeller on the flow field by means of a spatially and/or temporally varying force field is explored. Despite its simplicity, this model already appears to do a satisfactory job, because it generates statistical results, both mean flow and turbulence intensities, in close agreement with experimental data for the test case considered here. A major advantage of the model is that it allows in a straightforward way to evaluate different impeller shapes and tank geometries, and it permits scale-up studies of single-phase reactors. Because no information other than the impeller shape and its way of motion through the flow is required, such predictive studies can be realized. On the other hand, a disadvantage of the model is that the smallest scale of the impeller, here the thickness of its blades, must be at least of the order of the grid spacing. This condition may put a high demand on the resolution if this smallest scale is small compared to the diameter of the impeller and, the impeller, in turn, is small compared to the overall size of the reactor. Furthermore, in view of the strong "intermittent" behavior of the flow, especially in the vicinity of the impeller, more advanced subgrid-scale turbulence models, such as the dynamic SGS model or those accounting for stochastic backscatter, might do an even better job in simulations of this configuration. This issue will be addressed in the future. Nevertheless, it is clear from the present application that LES can be used to solve practical flow problems in engineering applications.

References

Bakker, R. A. 1995. Laser-Doppler measurements in a baffled stirred tank reactor with a disc turbine. Experimental data to appear in his Ph.D. thesis, Delft University of Technology, the Netherlands

Chen, S., Wang, J., Shan, X. and Doolen, G. 1992. Lattice-Boltzmann computational fluid dynamics in three dimensions. *J. Stat. Phys.*, **68**, 379

Eggels, J. G. M. and Somers, J. A. 1995. Numerical simulation of the free convective flow using the lattice-Boltzmann scheme. *Int. J. Heat Fluid Flow*, **16**, 357–364

Frisch, U., Hasslacher, B. and Pomeau, Y. 1986. Lattice gas automata for the Navier–Stokes equation, *Phys. Rev. Lett.*, **56** 1505–1508

Grötzbach, G. 1983. Spatial resolution requirements for direct numerical simulation of the Rayleigh–Bénard convection. *J. Comp. Phys.*, **49**, 241–264

d'Humières, D., Lallemand, P. and Frisch, U. 1986. Lattice gas models for 3-D hydrodynamics. *Europhys. Lett.*, **2**, 291–297

Kim, J., Moin, P. and Moser, R. 1987. Turbulence statistics in fully developed channel flow at low Reynolds number. *J. Fluid Mech.*, **177**, 133–166

Lyons, S. L., Hanratty, T. J. and McLaughlin, J. B. 1991. Large-scale computer simulation of fully developed turbulent channel flow with heat transfer. *Int. J. Numer. Methods Fluids*, **13**, 999–1028

Massaioli, F., Benzi, R. and Succi, S. 1993. Exponential tails in two-dimensional Rayleigh–Bénard convection. *Europhys. Lett.*, **21**, 305–310

McNamara, G. R. and Zanetti, G. 1989. Use of the Boltzmann equation to simulate lattice-gas automata. *Phys. Rev. Lett.*, **61**, 2332–2335

Rai, M. M. and Moin, P. 1991. Direct simulations of turbulent flow using finite-difference schemes. *J. Comp. Phys.*, **96**, 15–53

Ranade, V. V. and Joshi, J. B. 1990a. Flow generated by a disc turbine: Part I. Experimental. *Trans IChemE*, **68**, 19–33

Ranade, V. V. and Joshi, J. B. 1990b. Flow generated by a disc turbine: Part II. Mathematical modeling and comparison with experimental data. *Trans IChemE*, **68**, 34–50

Smagorinsky, J. 1963. General circulation experiments with the primitive equations: 1. The basic experiment. *Mon. Weather Rev.*, **91**, 99–164

Somers, J. A. and Rem, P. C. 1991. Flow computation with lattice gases. *Appl. Sci. Res.*, **48**, 391–435

Succi, S., Benzi, R., Vergassola, M. and Cancelliere, A. 1992. Hydrodynamic behavior of the lattice-Boltzmann equation. In *Numerical methods for the Simulation of Multiphase and Complex Flow*, Verheggen, T. M. M. (ed.), Lecture Notes in Physics, Vol. 398, Springer-Verlag, Berlin, 39–48

Wu, H. and Patterson, G. K. 1989. Laser-Doppler measurements of turbulent flow parameters in a stirred mixer. *Chem. Eng. Sc.*, **44**, 2207–2221